Nanoscale

Raman selection rule for surface optical phonons in ZnS nanobelts

Chih-Hsiang Ho,[a,b] Purushothaman Varadhan,[a] Hsin-Hua Wang,[a] Cheng-Ying Chen,[a] Xiaosheng Fang[c] and Jr-Hau He*[a]

We report Raman scattering results for high-quality wurtzite ZnS nanobelts (NBs) grown by chemical vapor deposition. In the Raman spectrum, the ensembles of ZnS NBs exhibit first order phonon modes at 274 cm^{-1} and 350 cm^{-1}, corresponding to A_1/E_1 transverse optical and A_1/E_1 longitudinal optical phonons, in addition to a strong surface optical (SO) phonon mode at 329 cm^{-1}. The existence of the SO band is confirmed by its shift with different surrounding dielectric media. Polarization dependent Raman spectra were recorded on a single ZnS NB and for the first time a SO phonon band has been detected on a single nanobelt. Different selection rules for the SO phonon mode are shown from their corresponding E_1/A_1 phonon modes, and were attributed to the breaking of anisotropic translational symmetry on the NB surface.

Introduction

Semiconducting nanomaterials provide new opportunities to exploit distinct properties from their bulk counterparts, making them potential candidates for near future electronic and optoelectronic applications.[1–3] These distinct properties not only bring possible breakthroughs in terms of device applications but also possess unique physical phenomena. For example, their large surface-to-volume ratio and local surface modulation of nanomaterials, leads to the observation of an extraordinary phonon mode known as surface optical (SO) phonon mode, which is not observed for their bulk counterparts.[4] Raman scattering, a non-destructive tool often used to investigate material properties such as composition or strain, has also been used to detect the SO phonon modes. Raman scattering has been employed to detect the SO phonon mode in various semiconductor nanostructures, including ZnS, ZnO, CdSe, GaP, GaAs and GaN.[4–12] However, an essential property of Raman scattering, the selection rule for the SO phonon mode, has not been widely observed for the single nanostructures, because of the poor signal to noise ratio and weak SO band as compared to their corresponding first order bands.

In this paper, we report the selection rule for Raman scattering for SO phonon modes in ZnS nanobelts (NBs) by polarization dependent Raman spectroscopy. The surface phonon modes in the Raman spectra were usually observed for an ensemble of nanostructures. Here, in order to understand the selection rule, we performed Raman scattering measurements on a single ZnS NB and successfully observed the SO phonon mode, which to the best of our knowledge, has never been seen in previous literature. The selection rule for the SO phonon mode was then found to be broken by the breaking of anisotropic translation symmetry on the surface.

Experimental section

The ZnS NBs were grown by a simple chemical vapor deposition method.[13] Highly pure ZnS powder (99.999%) and argon (Ar) gas was used as the source material and carrier gas respectively. ZnS powder was placed in an alumina boat and inserted into the center of the quartz tube. A Si wafer with 3 nm Au pre-deposited was placed downstream of the ZnS source. After purging the tube with Ar at 500 sccm (standard cubic centimeters per minute), the furnace temperature was ramped to 1100 °C and kept constant at this temperature for 30 minutes. After growth, the furnace was cooled down with a continuous flow of Ar.

The structural properties of as-grown ZnS NBs were characterized by X-ray diffraction, scanning electron microscopy (SEM), transmission electron microscopy (TEM) and Micro-Raman scattering. Micro-Raman scattering measurements were performed with backscattering geometry using a Jobin Yvon T6400 Raman spectrometer with a resolution of 0.3 cm^{-1}. A laser with wavelength of 532 nm was used as an excitation source and the laser beam was focused through a microscope with a spot size of about 1 μm in diameter. The

[a]Computer, Electrical and Mathematical Sciences and Engineering (CEMSE) Division, King Abdullah University of Science & Technology (KAUST), Thuwal 23955-6900, Saudi Arabia. E-mail: jrhau.he@kaust.edu.sa
[b]Electrical and Computer Engineering, Purdue University, West Lafayette, IN 47907, USA
[c]Department of Materials Science, Fudan University, Shanghai 200433, P. R. China

typical laser power at the surface of the NBs was 4 mW. A liquid nitrogen cooled charge coupled device was used to collect the scattered signal dispersed on 1800 grooves per mm grating. For Raman measurements of a single ZnS NB, the as-grown ZnS NBs on Si were sonicated in alcohol and dispersed on glass substrates.

Results and discussion

Fig. 1(a) shows the TEM image of the ZnS NBs dispersed on a copper grid and Fig. 1(b) shows the SEM image of ZnS NBs dispersed on Si substrates. Grown nanostructures have a belt-like morphology with typical dimensions of 0.5 μm in width and 50 nm in thickness. The length of the NBs varies up to few tens of micrometers. Fig. 1(c) shows the high resolution TEM (HRTEM) image with clearly resolved lattice arrangements, indicating high crystal quality of the as-grown ZnS NBs. The inset of Fig. 1(c) shows that the ZnS NBs are grown along the $(1\bar{1}00)$ direction and the inter-planar spacing values are found to be 3.3 Å and 6.3 Å corresponding to the $(1\bar{1}00)$ and (0001) crystal planes of wurtzite ZnS, which are close to the lattice constants of bulk wurtzite ZnS.[14] Selective area electron diffraction (SAED) also shows diffraction patterns with sharp fringes, confirming the high crystal quality of the ZnS NBs.

Wurtzite ZnS belongs to the space group C_{6v}^3 with two formula units per unit cell. As conventional group theory predicts, the wurtzite structure has several phonon modes including A_1, E_1, E_2 and B_1. A_1 and E_1 modes are both Raman and infrared spectra active, E_2 modes are Raman active and B_1 modes are optically silent. The A_1 phonon mode polarizes along the c-axis of the wurtzite structure while the E_1 mode polarizes perpendicular to the c-axis.[15,16] For wurtzite ZnS, A_1 and E_1 modes are reported to be nearly overlapped, which could be attributed to small the anisotropy of inter-atomic forces in ZnS.[17] Other than this, due to the small Bohr radius

of ZnS of around 2.5 nm, the phonon confinement effect is not expected in our ZnS NBs.[18]

The Raman spectrum collected from an ensemble of ZnS NBs is shown in Fig. 2. Each of the phonon wavenumbers is extracted by fitting the spectrum to a Lorentzian line shape. The peak at 350 cm^{-1} can be assigned to the E_1/A_1(LO) mode and the peak at 274 cm^{-1} can be assigned to the E_1/A_1(TO) mode.[5] The broad features at 350–450 cm^{-1} are related to the second-order Raman scattering, including combination and overtone of several ZnS phonon modes. The peak position of the ZnS bulk phonon modes is close to the reported bulk values, indicating the excellent crystal quality with strain-free growth of ZnS NBs.[5] The SO phonon modes are observed at 329 cm^{-1} with a stronger intensity than the corresponding E_1/A_1(LO) modes, which has been attributed to the high surface-to-volume ratio of the ZnS NBs. Note that SO phonon modes are usually weaker than related bulk modes and appear as a shoulder band.[4,6,19] However, in our case the SO phonon mode for the ensemble of NBs is stronger than for the LO and TO modes, encouraging us to investigate the SO phonon band in a single ZnS NB.

The SO phonon mode originates from the existence of an interface between materials with different dielectric constants (ε). The essential properties of SO phonon modes are that their peak position and line shape depends on the dielectric medium in contact with the surface. SO phonon modes have to be activated by a symmetry breaking mechanism associated with the modulation in the surface. It propagates along the interface and the amplitude decays exponentially into the bulk.[20] At the interface, the translational symmetry is broken due to surface roughness or geometrical dimension fluctuation made intentionally or unintentionally during the growth process.[4,6,21,22] The translational symmetry breaking gives additional crystal momentum that allows the transition of phonon mode away from the center of the Brillouin zone, which is not allowed in bulk material with perfect crystal symmetry due to momentum conservation. Therefore, nanomaterials with a large surface area provide much stronger SO phonon signals compared to the bulk phonon mode.
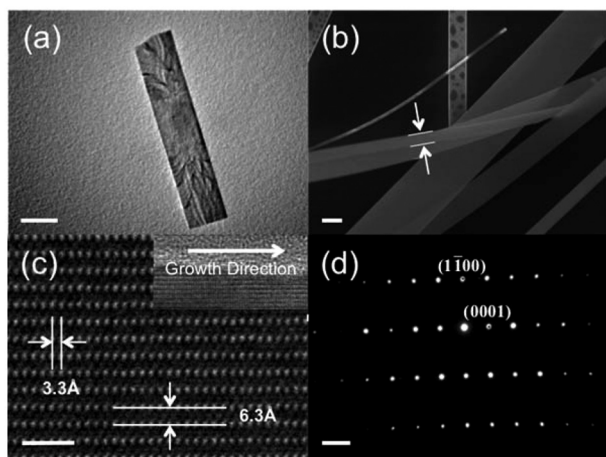

Fig. 1 (a) TEM image, (b) cross-sectional SEM image, (c) HRTEM image and (d) SAED of as-grown ZnS NBs. The scale bar is 0.5 μm for (a) and (b) and 2 nm for (c) and (d), respectively.
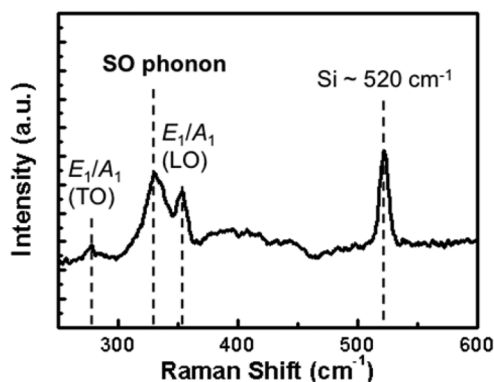

Fig. 2 Raman spectrum from an ensemble of ZnS NBs on Si substrate. The peak at 520 cm^{-1} is attributed to Si.

According to the dielectric continuum model, the dispersion relation of the phonon mode at the interface will be changed due to the different εs of the surrounding materials.[5,23] As a result, the wavenumber for the SO phonon mode (ω_{SO}) changes with the ε of the surrounding materials.

To confirm the existence of the SO phonon mode in the ZnS NBs, we compared the Raman spectra of samples immersed in air ($\varepsilon = 1$) and alcohol ($\varepsilon = 1.86$). As shown in Fig. 3a, ω_{SO} blue-shifts from 329 cm^{-1} to 326 cm^{-1} when immersed in alcohol while the bulk mode $E_1/A_1(LO)$ remains the same at 351 cm^{-1}. This result validates the assignment of the SO phonon mode at 329 cm^{-1}, demonstrating the surface-related characteristics of the SO phonon mode.

To further understand how the surface phonon mode is affected by the surrounding material, we employed the calculation describing the dispersion relation of SO phonon mode in ZnS NBs as an extreme case of a rectangular quantum wire.[23] Note that the calculation neglects the potential function describing the optical phonon mode at the corner and assumes the potential function is separable. By utilizing the electrostatic boundary condition, the dispersion relation of SO phonon is derived as below:

$$\varepsilon(\omega) \times \tanh(q_i L_i/2) + \varepsilon_s = 0, \tag{1}$$

$$\varepsilon(\omega) \times \coth(q_i L_i/2) + \varepsilon_s = 0, \tag{2}$$

where $\varepsilon(\omega)$ and ε_s are the dielectric constant of ZnS NBs and the surrounding material, respectively, ω is the related phonon wavenumber, q_i is the phonon wavevector and L_i is the feature size of the ZnS NBs. eqn (1) is the symmetric (S) mode and eqn (2) is the antisymmetric (AS) mode. By combining together the dielectric function and the Lyddane–Sachs–Tellar relation, we obtained the following dispersion relations of the SO phonon mode:[5]

$$\omega_{SO}{}^2(q)_s = \omega_{LO}{}^2 \times \left[\frac{\varepsilon_\infty \times (\varepsilon_0 \tanh(q_i L_i/2) + \varepsilon_s)}{\varepsilon_0 \times (\varepsilon_\infty \tanh(q_i L_i/2) + \varepsilon_s)}\right], \tag{3}$$

$$\omega_{SO}{}^2(q)_{AS} = \omega_{LO}{}^2 \times \left[\frac{\varepsilon_\infty \times (\varepsilon_0 \coth(q_i L_i/2) + \varepsilon_s)}{\varepsilon_0 \times (\varepsilon_\infty \coth(q_i L_i/2) + \varepsilon_s)}\right], \tag{4}$$

where ε_0 and ε_∞ are low and high frequency values of $\varepsilon(\omega)$. Based on these equations, we have calculated the dispersion relation of the SO phonon mode of ZnS NBs in air and alcohol as shown in Fig. 3b. In alcohol, the dispersion relation shifts to lower frequency at the region of higher crystal momentum and remains unchanged at the zone center of the Brillouin zone. The corresponding experimental ω_{SO} (Fig. 3a) in alcohol and air are labeled by the horizontal arrow and are found to intersect with the S mode branch, indicating SO phonon is in transverse mode. In accordance with the calculated dispersion relation, ω_{SO} is observed to shift to lower frequencies while the slight difference in wavevector q_i is attributed to the different spot that the Raman spectra was collected. It is also worth mentioning that for SO phonon in transverse mode with a given wavevector q_i, a larger feature size L_i, which denotes the direction SO phonon vibrates, leads to a higher ω_{SO}.

To gain insight into the selection rule for the SO phonon mode of ZnS nanostructures, we measured the polarization-dependent Raman spectrum of a single ZnS NB and the experimental setup is schematically shown in Fig. 4a. The polarization of incident light was varied from x to z direction while only the scattered light polarized in the z direction was collected. More specifically, the light configuration was changed from $Y(X,Z)$- to $Y(Z,Z)$-. The angle θ is defined as the angle between the x axis and the scattering polarization is changed from 0° to 90°. Polarization-dependent Raman spectra with four different angles are shown in Fig. 4b. The intensities of LO and SO phonon modes increase as the incident laser polarization changes from the x direction to the z direction.

The intensity ratio I_{SO}/I_{LO} as a function of θ is found to increase from 0.35 to 0.68 as θ changes from 0° to 90° (Fig. 4c). The peculiar difference in I_{SO}/I_{LO} with θ indicates that SO and LO phonon have different selection rules, which is not expected because the SO phonon mode originates from exactly the same atomic vibration as LO phonon modes even as θ changes. The selection rule that describes the polarization dependency of Raman scattering shows that the intensity of Raman scattering can be expressed as:
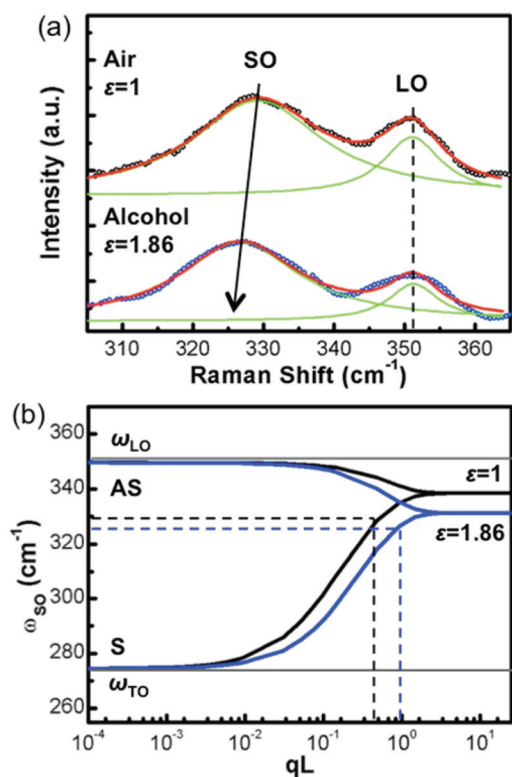

Fig. 3 (a) Raman spectra measured in the surrounding material with different dielectric constants (air and alcohol); (b) calculated SO phonon dispersion relation in air and alcohol. $q_i L_i$ is (the phonon wavevector) × (the feature size of the ZnS NBs).

$$I \propto \left|\overrightarrow{e_s} \times \overleftrightarrow{R} \times \overrightarrow{e_i}\right|^2 \tag{5}$$
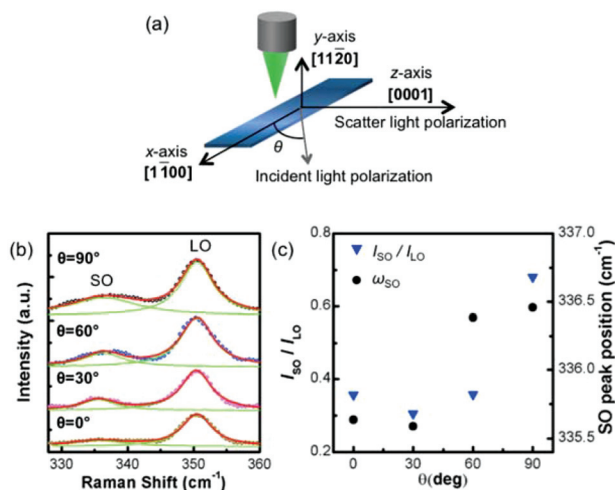
Fig. 4 (a) Schematic illustration of the polarization dependent Raman measurement. (b) Polarization dependent Raman spectra measured from a single ZnS NB with different angles. (c) Angular dependency of I_{LO}/I_{SO} and ω_{SO}. Single ZnS NB with different angles. (c) Angular dependency of I_{LO}/I_{SO} and ω_{SO}.

where I is the intensity, $\vec{e_s}$ and $\vec{e_i}$ are the polarization vectors of scattering light and incident light, respectively, and $\overleftrightarrow{R}$ is the Raman tensor. The Raman tensor of two vibration modes, A_1 and E_1 modes, of LO phonon can be expressed as[15]

$$E_1(x) = \begin{bmatrix} 0 & 0 & c \\ 0 & 0 & 0 \\ c & 0 & 0 \end{bmatrix} \quad (6)$$

$$A_1(z) = \begin{bmatrix} a & 0 & 0 \\ 0 & a & 0 \\ 0 & 0 & b \end{bmatrix} \quad (7)$$

where a, b, and c are constants related to electric polarizability. In this case, we have $\vec{e_s} = \hat{z}$ and $\vec{e_i} = \cos\theta\hat{x} + \sin\theta\hat{z}$, where $\hat{x}$ and $\hat{z}$ are the unit vectors along the x-axis and z-axis, respectively, as shown in Fig. 4a. The total intensity of the LO phonon mode (I_{LO}) can be derived as

$$I_{LO} = I_{A1} + I_{E1} = b^2 \sin^2\theta + c^2 \cos^2\theta = y_0 + a_0 \sin^2\theta,$$

where y_0 and a_0 are constants. As light configuration varies from $Y(X,Z)$- to $Y(Z,Z)$-, the allowed phonon mode is changed from E_1 to A_1 while the total intensity varies with $\sin^2\theta$, explaining the change of I_{LO} with θ. However, the SO phonon mode having the same vibration modes doesn't have the same selection rule so that I_{SO} becomes much stronger for $Y(Z,Z)$- than I_{LO}, indicating the A_1 vibration mode is amplified for the SO phonon. During the growth of NBs, growth condition in local regime continuously changes over time, inducing periodic surface roughness in the NB. As a result, surface roughening-induced translation symmetry breaking mostly occurs in the growth direction, which is the x-axis in our case.[4–6,21,22] Accordingly, we suggest that SO phonon modes are dominated by the phonon mode propagating along the x-axis, which is $A_1(TO)$ in this case. This inference is in accordance with our

calculated results as shown in Fig. 3b, that the SO phonon modes are in transverse mode. Moreover, the feature size L_x of the $A_1(TO)$ mode is several µm larger than the feature size L_z of the $E_1(TO)$ mode, which is around 500 nm. Therefore, according to the calculated dispersion relation in Fig. 3c, the SO phonon mode related to the $A_1(TO)$ vibration mode would have a larger q_iL_i that leads to a higher ω_{SO} as compared to the SO phonon mode related to $E_1(TO)$, which is in agreement with the variation of ω_{SO} as shown in Fig. 4c.

Conclusions

Wurtzite ZnS NBs with high crystalline quality were grown by the chemical vapor deposition. From Raman scattering measurements, we have observed a strong SO phonon mode in the ZnS NBs. The phonon wavenumber ω_{SO} is found to blue-shifted as the dielectric constant of surrounding material increases, confirming the presence of the SO phonon mode, which is in accordance with the calculation. Based on the polarization dependent Raman spectrum of a single ZnS NB, the selection rule of SO phonon is broken. The $A_1(TO)$ related SO phonon mode was found to dominate over the E_1 related SO phonon mode, which has been attributed to the anisotropy in breaking the translational symmetry arising from nano-structure growth.

Acknowledgements

Notes and references

1 Y. Huang, X. F. Duan and C. M. Lieber, *Small*, 2005, **1**, 142–147.
2 R. Agarwal and C. M. Lieber, *Appl. Phys. A: Mater. Sci. Process.*, 2006, **85**, 209–215.
3 X. F. Duan, Y. Huang, R. Agarwal and C. M. Lieber, *Nature*, 2003, **421**, 241–245.
4 R. Gupta, Q. Xiong, G. D. Mahan and P. C. Eklund, *Nano Lett.*, 2003, **3**, 1745–1750.
5 Q. H. Xiong, J. G. Wang, O. Reese, L. C. L. Y. Voon and P. C. Eklund, *Nano Lett.*, 2004, **4**, 1991–1996.
6 S. Bhattacharya, A. Datta, S. Dhara and D. Chakravorty, *J. Raman Spectrosc.*, 2011, **42**, 429–433.
7 Y. F. Huang, S. Chattopadhyay, H. C. Hsu, C. T. Wu, K. H. Chen and L. C. Chen, *Opt. Mater. Express*, 2011, **1**, 535–542.
8 D. Fan, R. Zhang, Y. Zhu and H. Peng, *Physica B*, 2012, **407**, 3510–3514.
9 R. Mata, A. Cros, K. Hestroffer and B. Daudin, *Phys. Rev. B: Condens. Matter*, 2012, **85**, 035322.

10 I. M. Tiginyanu, A. Sarua, G. Irmer, J. Monecke, S. M. Hubbard, D. Pavlidis and V. Valiaev, *Phys. Rev. B: Condens. Matter*, 2001, **64**, 233317.

11 G. D. Mahan, R. Gupta, Q. Xiong, C. K. Adu and P. C. Eklund, *Phys. Rev. B: Condens. Matter*, 2003, **68**, 073402.

12 H. Lange, M. Artemyev, U. Woggon and C. Thomsen, *Nanotechnology*, 2009, **20**, 045705.

13 Q. Li and C. R. Wang, *Appl. Phys. Lett.*, 2003, **83**, 359–361.

14 R. R. Reeber and G. W. Powell, *J. Appl. Phys.*, 1967, **38**, 1531.

15 C. A. Arguello, D. L. Rousseau and S. P. S. Porto, *Phys. Rev.*, 1969, **181**, 1351.

16 H. Harima, *J. Phys.: Condens. Matter*, 2002, **14**, R967–R993.

17 R. Loudon, *Adv. Phys.*, 1964, **13**, 423–482.

18 R. Rossetti, R. Hull, J. M. Gibson and L. E. Brus, *J. Chem. Phys.*, 1985, **82**, 552–559.

19 D. Spirkoska, G. Abstreiter and A. F. I. Morral, *Nanotechnology*, 2008, **19**, 435704.

20 K. W. Adu, Q. Xiong, H. R. Gutierrez, G. Chen and P. C. Eklund, *Appl. Phys. A: Mater. Sci. Process.*, 2006, **85**, 287–297.

21 S. Sahoo, S. Dhara, A. K. Arora, R. Krishnan, P. Chandramohan and M. P. Srinivasan, *Appl. Phys. Lett.*, 2010, **96**, 103113–103113.

22 J. H. Zhu, J. Q. Ning, C. C. Zheng, S. J. Xu, S. M. Zhang and H. Yang, *Appl. Phys. Lett.*, 2011, **99**, 113115–113113.

23 M. A. Stroscio, K. W. Kim, M. A. Littlejohn and H. H. Chuang, *Phys. Rev. B: Condens. Matter*, 1990, **42**, 1488–1491.